Journal of Alloys and Compounds 509 (2011) 7330–7336

Contents lists available at ScienceDirect

Journal of Alloys and Compounds

journal homepage: www.elsevier.com/locate/jallcom

Aging process of photosensitive chalcogenide films deposited by electron beam deposition

F. Charpentier[a], M. Dussauze[b], M. Cathelinaud[c], G. Delaizir[a], E.I. Kamitsos[b], J.-L. Adam[a], B. Bureau[a], V. Nazabal[a,*]

[a] Sciences Chimiques de Rennes, UMR6226, Université Rennes 1, 35042 Rennes, France
[b] Theoretical and Physical Chemistry Institute, National Hellenic Research Foundation, Athens, Greece
[c] Mission des Ressources Et compétences Technologiques, UPS2274 92135 Meudon, France

ARTICLE INFO

Article history:
Received 30 January 2011
Received in revised form 2 April 2011
Accepted 10 April 2011
Available online 16 April 2011

Keywords:
Thin film
Chalcogenide
Evaporation
Aging
Photosensitivity
Coating
Optical waveguide

ABSTRACT

Chalcogenide films attract broad interest due to their use as optical components like narrow band-pass filters, omnidirectional reflectors cladding, all-optical signal processing devices or optochemical sensors. $Ge_{15}Sb_{20}S_{65}$ and $As_{30}Se_{50}Te_{20}$ chalcogenide amorphous films were deposited by electron beam deposition (EBD) using their corresponding bulk glasses as targets. The structure of both bulk and thin film has been studied by far-IR and Raman spectroscopy. This study investigated an ordinary aging behavior of the chalcogenide films by exposing them to natural light under atmospheric conditions for a period of six months. Both films were found to be photosensitive as manifested by the shift of their optical band-gap to shorter or longer wavelength depending on chemical composition. Aging was found to induce also morphological changes, most notably the likely growth of arsenic trioxide microcrystals on the surface of $As_{30}Se_{50}Te_{20}$ films. Such effects were discussed in terms of photo-oxidation and photo-hydrolysis phenomena, the extent of which was found to be relatively limited for $Ge_{25}Sb_{10}S_{65}$ films. The larger stability of the latter films against crystal growth at the surface was associated with the ability of germanium to bond to diffusing oxygen atoms in germanium-oxysulfide tetrahedral arrangements.

1. Introduction

Chalcogenide (Chg) films are the subject of numerous studies because of their possible applications in the field of optical coatings – such as manufacturing of narrow bandpass filters (NBFs) in the near infrared and mid-infrared region or special applications in the infrared range [1,2] – or omnidirectional reflector cladding [3,4] and in opto-chemical sensors [5,6] while all-optical signal processing involving the control of light by light through nonlinear effects [7,8] can be foreseen for such films. In this work, we are interested in the evolution with time of chalcogenide films developed by electron beam deposition. This technique is known to be suitable for manufacturing thick and homogeneous films that can fulfil size requirements set by special applications.The two chalcogenides glass compositions selected for this study, $Ge_{15}Sb_{20}S_{65}$ (2S1G) and $As_{30}Se_{50}Te_{20}$ glass (TAS), combine remarkable properties of chalcogenide materials; (i) direct evaporation from a glass target with retention of the initial stoichiometry, (ii) large optical window covering the spectral region from 500 nm to 11 μm for 2S1G film and from 1 μm to 18 μm for TAS film, (iii) high refractive index at 1540 nm (2.425 for 2S1G, and 2.871 for TAS films with thickness of 1.55 μm) [9], and (iv) photosensitivity [2,10]. Chalcogenide materials are known to be photosensitive, as well as sensitive to oxygen and humidity, all these phenomena leading to changes in optical properties and film morphology. Evaporated Chg films can manifest shifts of their optical absorption edge toward longer or shorter wavelengths (photodarkening and photobleaching, respectively), and modifications of their refractive index under light irradiation with appropriate energy and intensity [11]. Such photoinduced effects on physicochemical properties of chalcogenide glasses and films can be related to modifications of their electronic/atomic structure. Additionally, chalcogenide films and fibers with a surface to volume ratio higher than that of bulk materials can exhibit surface alterations due to crystallisation induced by oxidation. This behavior depends strongly on the type of chemical system, the specific composition and the employed deposition method. The formation of As_2O_3 microcrystals at the surface of $As_2S(Se)_3$ based glass has been reported by many authors [12–15]. Consequently, the optical property control of chalcogenides thin films, which is necessary for technological applications, requires a better understanding of their glass network structure and the assessment of a natural aging effect on their optical and

* Corresponding author.
E-mail address: virginie.nazabal@univ-rennes1.fr (V. Nazabal).

0925-8388/$ – see front matter © 2011 Elsevier B.V. All rights reserved.
doi:10.1016/j.jallcom.2011.04.054

morphological characteristics which could be detrimental for a variety of applications.

2. Experimental method

2.1. Glass target synthesis

Chalcogenide glasses of composition $Ge_{15}Sb_{20}S_{65}$ (2S1G) and $As_{30}Se_{50}Te_{20}$ (TAS) were prepared in the form of rods from the appropriate amounts of high-purity commercial elements (99.999%). Chemical elements like Ge and Sb are used as such without additional purification by selecting pieces without traces of surface oxidation. While elements as As, S, Se, and Te were specially purified to remove oxygen, molecular water, carbon and silica. These impurities introduce absorption in the mid- and far-IR ranges, as well as bulk scattering losses due to micro-inclusions. The chemical reagents S and Se were purified by vacuum distillation with a low rate of evaporation. The synthesis reactor was evacuated in an oil-free vacuum (10^{-2} Pa). Then, the sealed silica ampoule containing the reagents was placed into a rocking furnace heated at 850 °C for 12 h for 2S1G (650 °C for 8 h for TAS) and quenched in water. In a final stage, the prepared chalcogenide samples were annealed for 4 h at temperatures close to glass transition temperature and then cooled slowly to room temperature. The glass samples were obtained as rods with diameter of 18 mm and length of approximately 50 mm. Several glass cylinders were obtained from the same batch, allowing great reproducibility between successive EBD depositions.

2.2. Deposition method

Typical equipment of electron beam deposition (EBD) used for the preparation of coatings was a Balzers BAK 600 evaporation plant with a 60-cm stainless steel bell jar and two electron beam guns with water-cooled crucibles. TAS and 2S1G materials were placed in graphite crucibles of 4-cm^3 capacity. An *x–y* sweep could be used to increase the film uniformity. The film was deposited on fused silica or silicon substrates, having all both surfaces optically polished, that were subjected to a normal cleaning procedure prior to being cleaned by a discharge in vacuum chamber. The distance from the source to substrates was around 50 cm. Controlled by a quartz sensor, deposition took place at a rate of 1 nm/s with a pressure of 2×10^{-4} Pa. The total thickness of single TAS and 2S1G layer was about 1.5 and 5 μm monitored by optical transmittance method. After deposition optical constants – refractive index (n) and extinction coefficient (k), uniformity were determined by spectrophotometry method at room temperature, in spectral range 0.5–1.6 μm.

2.3. Characterisation of bulk glasses and films by Raman and infrared spectroscopy

Infrared measurements were performed on 2S1G and TAS bulk glasses and EBD films at room temperature on a Fourier-transform vacuum spectrometer (Bruker 113v), equipped with two sources (globar and Hg arc), two detectors (DTGS with KBr and polyethylene windows) and five different beam splitters, KBr for the mid-IR and four mylar films for the far-IR (with thickness 3.5–25 μm), to cover the frequency range from 30 to 5000 cm^{-1}. Each spectrum results from the average of 400 scans measured with a typical resolution of 2 cm^{-1}. The infrared spectra of bulk glasses were recorded in the reflectance mode at quasi normal incidence (11°), and the complex refractive index of each sample was obtained through Kramers–Krönig analysis of its specular reflectance spectrum [16,17]. The infrared spectra reported in this work are in the form of absorption coefficient spectra, $\alpha(\nu)$, calculated from the relation $\alpha(\nu) = 4\pi\nu k(\nu) = 2\pi\nu\varepsilon''(\nu)/n(\nu)$, where $n(\nu)$ and $k(\nu)$ are the real and imaginary parts, respectively, of the complex refractive index, $\varepsilon''(\nu)$ is the imaginary part of the dielectric function and ν (in cm^{-1}) is the infrared frequency.

Thin films were deposited on infrared-transparent silicon wafers (1 0 0 orientation) having both surfaces optically polished. Infrared transmittance spectra of thin films were measured at low resolution (10 cm^{-1}) in order to average experimentally the interference pattern due to multiple internal reflections in the silicon substrate. A systematic comparison was made between the infrared spectra measured for thin films and corresponding spectra calculated using the infrared response functions (n, k) of bulk glassy targets and Si substrate. To this aim, we made use of a model based on rigorous expressions for transmittance of a film/substrate bilayer system which takes into full account all optical effects occurring in such a system. The model relevant to the present study is reported elsewhere [18–20].

Raman spectra were recorded at room temperature on a confocal micro-Raman instrument (Renishaw) in the backscattering geometry, using the 785 nm excitation line of a solid state laser and typical resolution of 3 cm^{-1}. The spectrophotometer includes a holographic Notch filter for Rayleigh rejection, a microscope equipped with a 100× objective, and a CCD air cooled detector.

2.4. Aging study

For each chalcogenide film composition, the influence of natural light exposure and humidity was considered. Thus, some EBD films were stocked under atmospheric conditions while other films were protected from light by keeping them in dark, or were protected from humidity by placing them in a glove-box under argon atmosphere (few ppm of [H_2O]). The 2S1G and TAS thin films deposited on fused silica substrate were used to probe optical alterations in the visible–near-infrared spectral domain. Transmission curves of one layer for 2S1G and TAS were recorded just after deposition and after 1, 3 and 6 months using a visible–near-infrared spectrophotometer for each chalcogenide material. For morphological studies, chalcogenide films deposited on silicon substrates were analysed by field emission scanning electron microscopy (JEOL 6301F) at various times of the aging study.

Table 1
Chemical composition by EDS of 2S1G and TAS bulk glass and EBD films.

Element		Bulk (±0.5 at.%)	EBD film (±0.5 at.%)	
			1.5 μm	5 μm
2S1G	Ge	15.0	15.3	14
	Sb	21.2	22.5	25.6
	S	63.9	62.2	60.4
TAS	Te	20.3	19.8	21.5
	As	29.4	30.9	29.8
	Se	50.2	49.3	48.7

3. Results and discussion

3.1. Chemical compositions

The composition of EBD films with thicknesses 1.5 and 5 μm and of the bulk targets is listed in Table 1. The values reported are undoubtedly representative of compositions of EBD films; the compositions do not fluctuate much between films with comparable thickness. For 2S1G films with thickness of about 1.5 μm, the chemical composition was very close to that of the bulk glass. The noted sulfur deficiency (2 at.%) is usual for sulfide films, and this is due to the higher volatility of sulfur in comparison to other elements. Relative to sulfur, an increase in the antimony content was observed (1 at.%). For thicker films, the composition changes were more pronounced. The ratio of S/(Ge + Sb) decreased by 7% (14% for 5 μm film) and the ratio Sb/Ge increased slightly (4%), this effect being larger for the 2S1G 5 μm film. Considering the EDS accuracy of ±0.5%, the composition of TAS films was very close that of the bulk glass target regardless of film thickness. It is noted that for this specific composition the melting or evaporation is congruent, and this leads to film with compositions comparable to that of the bulk material.

3.2. Structural characterization by Raman and IR spectroscopy

Even if the composition of films is not removed from those of the bulk counterparts, it is necessary to characterise the structural organisation of the as-evaporated films which may differ from that of bulk glasses. As a matter of fact, after condensation on a cold substrate of the vapours formed during evaporation, non-homogeneous films in a very small scale are usually obtained for as-evaporated films compare to bulk. The chemical reaction between evaporated molecules and atoms is certainly slow down under low temperature deposition on substrate inducing an amorphous structure highly influenced by the method of deposition. To describe with confidence the structure of as-evaporated films, two series of glasses has been studied to identify the changes in relative intensity and/or shift of the vibrational bands versus their variations in composition.

3.2.1.1. Structure of Ge–Sb–S bulk glasses and 2S1G films

Fig. 1(a) and (b) presents the Raman and IR spectra of bulk glasses with composition GeS_2, $Ge_{25}Sb_{10}S_{65}$ and $Ge_{15}Sb_{20}S_{65}$ (2S1G). Before discussing the vibrational spectra of glass 2S1G it is useful to review briefly the vibrational characteristics of the GeS_2 glass [21–24]. Considering the structural unit $GeS_{4/2}$ (tetrahedral entities with four bridging sulfur atoms), one can assign the

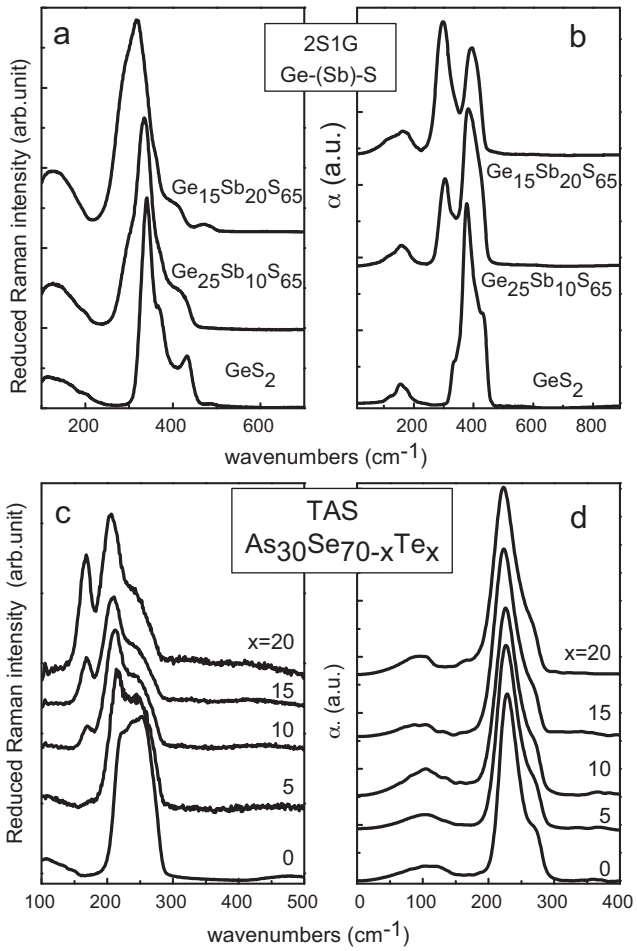

Fig. 1. Raman (a and c) and Far-IR (b and d) spectra obtained on bulk Ge–Sb–S and As–Se–Te glasses.

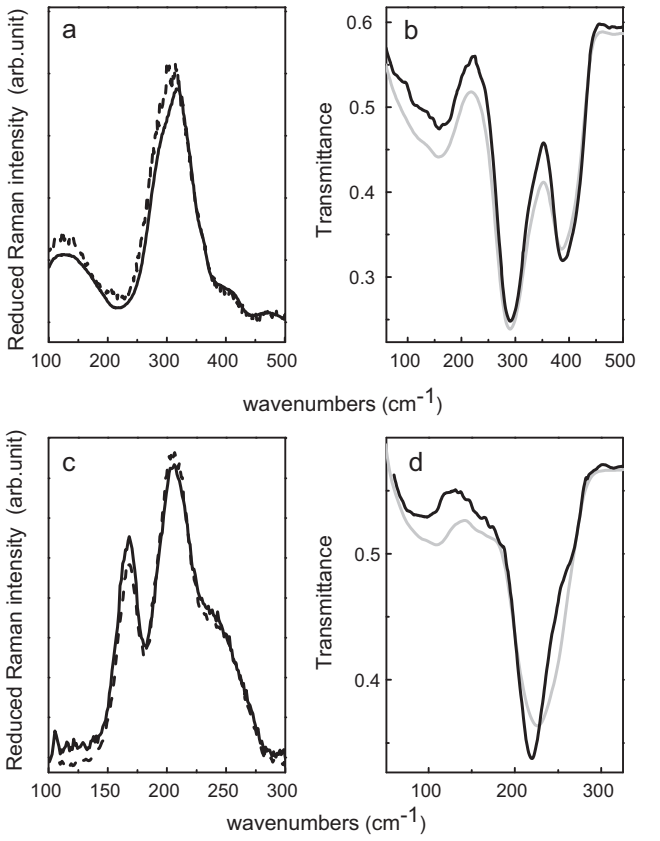

Fig. 2. Raman spectra (a and c) of and bulks (black lines) and thin films (dashed lines) deposited by EBD on silicon substrates. Measured infrared transmittance spectra (b and d) for $Ge_{15}Sb_{20}S_{65}$ (3 μm) and $As_{30}Se_{50}Te_{20}$ (6 μm) films (gray lines,). The black lines show calculated FIR spectra (b and d).

340 cm^{-1} band to the $GeS_{4/2}$ symmetric stretching mode (ν_1) active mainly in Raman, and the 370 cm^{-1} band to its asymmetric stretching mode (ν_3) active mainly in the IR. The $GeS_{4/2}$ bending modes ν_2 and ν_4 are active in both IR and Raman at 115 and 150 cm^{-1}, respectively. The Raman peak at 370 cm^{-1} is called usually "companion peak", ν_{1c}, is has been attributed also to germanate tetrahedral units linked by edges [21]. The Raman and IR activities at higher frequencies (420–430 cm^{-1}) have been related to vibration of tetrahedral units linked by S–S bridges [25].

Addition of antimony to GeS_2 induces the appearance of strong vibrational modes around 290 cm^{-1} in both Raman (shoulder) and IR (main peak) spectra. With reference to reports for Sb_2S_3 thin film [26,27] and for As_2S_3–Sb_2S_3 and Ge–Sb–S glasses [9,28], the band at ca. 290 cm^{-1} can be associated with the asymmetric stretching mode (ν_3) of [$SbS_{3/2}$] trigonal pyramids. The symmetric stretching mode, ν_1, of [$SbS_{3/2}$] pyramids should be related to the strongest Raman peak of glass 2S1G at 318 cm^{-1} (Fig. 1(a)). Also, the second strongest IR band 2S1G at 395 cm^{-1} (Fig. 1(b)) could be attributed to the asymmetric stretching mode, ν_{as}, of mixed Ge–S–Sb bridges. The low frequency region of Raman and IR spectra associated with bending modes (80–250 cm^{-1}), appears to become broader and to gain relative intensity with increasing Sb content.

The Raman and IR spectra of 2S1G thin film and bulk glass are compared in Fig. 2(a) and (b), respectively. As noticed in Section 2, the spectral comparison in the IR is based on a calculated transmittance spectrum which integrates all optical effects occurring in a bilayer system (film and substrate) [18–20]. Both figures demonstrate spectral variations between bulk glass and film. The 2S1G film Raman spectrum presents a slight shift of the most intensive band to lower frequency (310 cm^{-1}), and an increased intensity of the low frequency envelope (130 cm^{-1}). The appearance of a weak band at ca. 208 cm^{-1} can be also noted, while no change is observed for the band at 475 cm^{-1}. The IR spectra show change in relative intensity of the two principal bands at ca. 290 and 388 cm^{-1} and a gain in intensity of the low frequency band (156 cm^{-1}). In line with the assignments discussed above, we attribute these Raman and IR trends to an increased content of film in $SbS_{3/2}$ pyramidal units relative to the bulk target. This result agrees well with the composition changes induced by the EBD technique (Table 1), where for the 5 μm film the Sb/Ge ratio is 1.83 as compared to 1.42 for the bulk glass. The slight deficiency of films in sulfur could be compensated by formation of homopolar bonds like Ge–Ge and Sb–Sb [26].

3.2.2. *Structure of $As_{30}Se_{70-x}Te_x$ bulk glasses and $As_{30}Se_{50}Te_{20}$ film*

Bulk glasses in the system $As_{30}Se_{70-x}Te_x$ present an excess of Se and Te compared to the stoichiometric $As_{40}Se_{60-x}Te_x$ compositions [29]. Thus, the interconnection of $AsX_{3/2}$ pyramidal units (with X being either Se or Te) should incorporate some Se–Se, Se–Te or Te–Te bonds. In addition, formation of rings or chains including both Se and Te could be possible. Fig. 1(c) and (d) presents the Raman and IR spectra of bulk glasses in the system $As_{30}Se_{70-x}Te_x$ from $x = 0$ to $x = 20$. For the bulk $As_{30}Se_{70}$ composition, we expect a glass network composed mainly of [$AsSe_{3/2}$] pyramidal units. According to Lucovsky [30,31], the IR bands at 230 and 110 cm^{-1} could be assign to the asymmetric stretching (ν_3) and to the bending (ν_2) modes, respectively, of [$AsSe_{3/2}$] pyramids, while the symmetric stretching vibration of [$AsSe_{3/2}$] pyramids (ν_1)

is expected at ca. 225 cm^{-1} in the Raman spectrum. The excess of Se would induce the formation of –Se–Se– bonding in various arrangements including As–Se–Se–As bridges, Se_8 rings and Se_n chains. With reference to previous works of Lucovsky [31,32] and Ohsaka [33] on pure vitreous selenium, Mori et al. [34] on the system As–Se, and Iovu et al. on $As_xSe_{(100-x)}$ glasses with $x = 0$ to $x = 40$ [35], we attribute the high frequency IR components at ca. 260 cm^{-1} and the Raman one at 252 cm^{-1} to Se_8 rings. The main mode linked to Se_n chains is expected at 238 cm^{-1} in the Raman, and this might be part of the broad band observed from 200 to 280 cm^{-1} in the Raman spectrum of As_3Se_7 glass. Also, a Raman contribution of As–Se–Se–As entities is expected at ca. 270 cm^{-1}.

Upon substitution of Se by Te, the high frequency components around 250–270 cm^{-1} appear to loose gradually intensity in both Raman and IR spectra (Fig. 1(c) and (d)), and this demonstrates the progressive destruction of Se–Se bridges. In the Raman spectrum, two intensive bands develop at 168 and 205 cm^{-1} and become the main features of the $x = 20$ glass. The IR spectrum of the $x = 20$ glass shows its main band at 220 cm^{-1}. We attribute the Raman band at 205 cm^{-1} to vibrations of Se–Te bonds as observed in the system $Se_{1-x}Te_x$ [36] or to As–Se vibration in mixed $AsSe_{3-x}Te_x$ units [37,38]. The strong IR band at 220 cm^{-1} would be consistent with the formation of mixed $AsSe_{3-x}Te_x$ units, considering that the ν_3 mode of $[AsSe_{3/2}]$ pyramids is active at 230 cm^{-1} (Fig. 1(d)). The Raman band at 168 cm^{-1} could be related to As–Te stretching in $AsSe_{3-x}Te_x$ entities [37,38].

In Fig. 2(c) and (d), the Raman and IR spectra of TAS thin film and bulk glass are compared. The Raman spectra show a change in relative intensity between the two strong bands at 170 and 205 cm^{-1}, while the strongest IR band shifts from 220 to 226 cm^{-1} from the bulk glass to thin film state. A similar shift from 95 to 105 cm^{-1} is observed for the infrared active bending modes. Recalling that the ν_3 and ν_2 modes of $[AsSe_{3/2}]$ pyramids appear at 230 and 110 cm^{-1}, respectively, the observed IR trends suggest that the TAS film is relatively enriched in As–Se bonds and deficient in As–Te bonds compared to its bulk glass target. Also, the intense IR band at 226 cm^{-1} for the film appears broader toward higher frequency when compared to the 220 cm^{-1} band of the bulk. This may indicate replacement of Se_8 rings in the bulk glass by new ring arrangements in the film involving also Se–Te bonds [33]. The observed trends in the infrared spectra are consistent with the manifested intensity variations of the Raman bands at 170 and 205 cm^{-1} when changing from bulk to thin film state. As seen in Table 1, the chemical composition of the film measured by EDS shows a slight increase in the Te content relative to bulk glass. This result would be consistent with the observed Raman and IR spectral variations provided that the involvement of Te in Se–Te bonding is enhanced upon film formation.

To summarize the results for TAS compositions we note that after EBD deposition (i) chemical analysis shows a slight increase in the tellurium content, and (ii) vibrational spectroscopy suggests a decrease in the number of As–Te bonds in favor of As–Se and Se–Te bonding (with bond energies really close: As–Te = 205 kJ/mol and Se–Te = 195 kJ/mol). Thus, Te atoms are preferentially bonded to Se atoms in the film than in the bulk, and this reduces the proportion of As–Te–As bonds in mixed $AsSe_{3-x}Te_x$ entities. Additional analyses are in progress to confirm these first conclusions.

3.3. Optical natural aging effects

Absorption measurements of TAS and 2S1G films deposited on fused silica substrates were performed in the visible–near infrared region to probe the evolution of the optical band-gap during a 6-months aging experiment. The analysis of the optical absorption coefficient data, $\alpha(\nu)$, indicates that the optical band-gap, E_{opt}, of

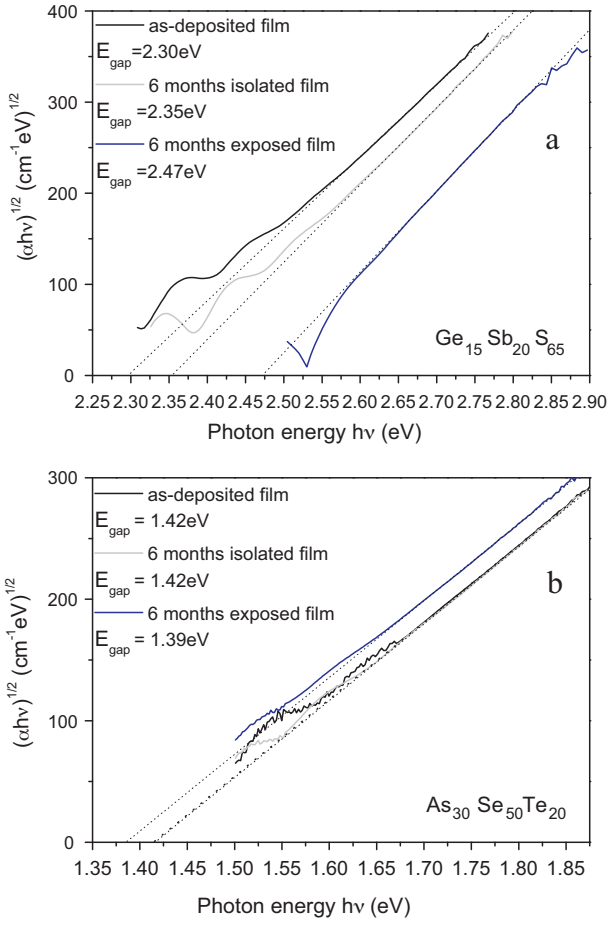

Fig. 3. $(\alpha h\nu)^{1/2}$ versus $(h\nu)$ of $Ge_{15}Sb_{20}S_{65}$ (a) and $As_{30}Se_{50}Te_{20}$ (b) EBD film as-deposited and exposed to light and air atmosphere or darkness and Argon atmosphere.

these films obeys the Tauc's relationship for the allowed indirect transition [39],

$$\alpha(\nu) = \delta \frac{(h\nu - E_{opt})^2}{h\nu} \quad (1)$$

where $h\nu$ is the photon energy and δ is a constant which depends on the transition probability. The extrapolation of the linear portion of Tauc's plots to $(\alpha h\nu)^{1/2} = 0$ yields the values of the optical band-gap [40]. Fig. 3 represents plots of $(\alpha h\nu)^{1/2}$ versus $(h\nu)$ for the as-deposited chalcogenide films TAS and 2S1G, after 6 months of exposure to natural light in air atmosphere, and after staying for 6 months in dark under argon atmosphere. As seen in Fig. 3, measurements of the as-deposited films resulted in $E_{opt} = 1.42 \pm 0.01$ eV for TAS and $E_{opt} = 2.30 \pm 0.01$ eV for 2S1G. After one month, the transmission curve of 2S1G film was shifted slightly toward shorter wavelengths while the curve of TAS films was shifted toward longer wavelength. After 6 months under atmospheric conditions, the optical band-gap value was 1.39 ± 0.01 eV and 2.47 ± 0.01 eV for TAS and 2S1G films, respectively. The optical band-gap values determined for the two aging experiments are collected in Table 2. For the protected TAS film (in dark under argon atmosphere), it was found that aging leaves practically unaffected the optical band-gap, while a small decrease of E_{opt} was observed after exposure to atmospheric conditions. We found that an ordinary aging had a stronger effect on optical properties of 2S1G film as manifested by the E_{opt} increase with aging time. This effect was more pronounced for the film exposed to atmospheric conditions. The variation in band-gap energy of as-deposited chalcogenide EBD films

Table 2
Optical band gap values for intermediary step of aging experiments for 2SG (1.7 ± 0.1 μm) and TAS (1.5 ± 0.1 μm) films.

	Exposed to atmospheric conditions		Isolated from light and humidity	
	2S1G (±0.01 eV)	TAS (±0.01 eV)	2S1G (±0.01 eV)	TAS (±0.01 eV)
t_0 – as deposited	2.30	1.42	2.30	1.42
t_1 – 1 month	2.36	1.37	2.32	1.42
t_2 – 3 months	2.37	1.39	2.32	1.42
t_3 – 6 months	2.47	1.39	2.35	1.42

submitted to illumination of xenon arc lamp under air atmosphere have been already observed with a photobleaching of $Ge_{15}Sb_{20}S_{65}$ film and photodarkening of $As_{30}Se_{50}Te_{20}$ film [2,41].

Generally for studies concerning the effect on optical properties of as-evaporated films submitted to light exposure close to band-gap energy, irreversible photoinduced changes occurs and it is usually suggested that heteropolar bonds creation and homopolar bond break are involved. Indeed, the energies of the homopolar and heteropolar bonds are not removed in the range of ~50–80 kJ/mol enabling the coordination changes of atoms [42]. These phenomena generally result, for films close to or over stoichiometry with higher proportion of chalcogen, in a photodarkening effect of the As-based films and a photobleaching behavior of the Ge-based films for film rich in chalcogen or close to stoichiometry. From literature, it is interesting to note that the addition of As into Ge–S films alters the character of photoinduced changes following a progressive modification of ΔE_{opt} from photobleaching to photodarkening [43]. It is reasonable to assume that photo-induced changes like those described above are associated with microstructural rearrangement which can affect the optical band-gap [44]. Therefore, the photodarkening and photobleaching are usually related to the formation or vanishing of defects and localised electronic states in the tails of conduction and valence bands, which reduce or increase the energy band-gap, respectively.

The Se and Te chalcogens with a high electronic lone pair density are usually involved in the coordination change to form new bonds in As based glass system. This ability makes the photosensitive relaxation easiest for $As_{30}Se_{50}Te_{20}$ films submitted to natural light leading to photodarkening effect for such composition ($\Delta E_{opt} = -0.03$ eV).

In as-evaporated thin films of the system Ge–Sb–S, photobleaching and photodarkening can be observed after exposure [10]. In our case as the content of antimony is lower than 2/3, a photobleaching effect can be expected considering the relaxation of the structure. During the evaporation process of Ge–Sb–S glass target, GeS_x ($x < 2$) and S_2 or S_8 molecules may be formed by dissociation of GeS_2 vapours leading to some inhomogeneity in the as-evaporated films. The relaxation of the film facilitated by exposure may enable the formation of GeS_2 from these fragments; even if it was not clearly detectable by Raman or IR spectroscopy. Thus, a shift of the E_{opt} band-gap toward shorter wavelengths can be explained as the E_{opt} of GeS_2 is higher than those of Ge_2S_3 or GeS getting to a photobleaching of the $Ge_{15}Sb_{20}S_{65}$ as-evaporated film [45].

Additionally, photo-induced phenomena leading to changes of optical parameters may be also caused by photo-oxidation under the influence of atmosphere. While the mechanism of photo-oxidation of chalcogenides is still under discussion, previous works [46–51] suggest that photo-induced changes may be due to incorporation of oxygen in the glass matrix and to formation of covalent bonds with glass-forming elements, e.g. Ge–O or Ge–OH bonds at the surface in the case of Ge–Sb–S films. It should be noted that the formation of oxygen bonds with germanium is mostly irreversible in sulfide and selenide films. As shown in Table 2, the optical band-gap value of the 2S1G changes by $\Delta E_{opt} = +0.05$ eV even after protection in the dark under argon atmosphere. It is noted that the H_2O content was carefully controlled and limited around 3–5 ppm, whereas oxygen was not purified in the glove box. Thus, we can certainly expect a better E_{opt} keeping by limiting the oxygen content. As a result, we assume that such a photo-oxidation mechanism is certainly predominant for the as-deposited 2S1G film (15 at.% Ge).

However, the same aging conditions in the dark under argon atmosphere did not affect the optical behavior of TAS with its optical band-gap value remaining constant within ±0.01 eV variation. This suggests that film of the system As–Se–Te seems to be less sensitive to oxygen than that of Ge–Sb–S system. More precisely, the diffusion of oxygen into the network and reaction at the surface to form new mixed oxysulfide entities might be more efficient in Ge–Sb–S films. As a result, the band-gap of 2S1G film is shifted to higher energy as expected considering a transition to larger band-gap energy like for germanium oxide system concomitantly of the diminution of homopolar and dangling bonds well known to decrease band-gap energy in Ge based as-evaporated films. Nevertheless, the natural relaxation of the film can also contribute to the photobleaching and the presence of Ge–Ge and Sb–Sb homopolar bonds in as-deposited 2S1G films have been confirmed by vibrational spectroscopies as described previously in structural approach.

The $As_{30}Se_{50}Te_{20}$ and $Ge_{15}Sb_{20}S_{65}$ films were studied after aging without clear conclusions can be drawn from this analysis. It does not seem that significant changes in the glass network structure take place during a natural aging at least unambiguously detected by these techniques.

3.4. Morphological aging effects

TAS and 2S1G films deposited on silicon were cleaved for morphological characterisation by SEM. The surface of these samples was observed after one, three and six months of aging under different conditions of light exposure and humidity. Fig. 4 presents SEM images of TAS and 2S1G films as-deposited by EBD (Fig. 4(a)), and after 6-months exposure to light under air atmosphere (Fig. 4(b)), or to darkness under argon atmosphere (Fig. 4(c)). Considering cleavage effects, Fig. 4(a) shows clearly that the as-deposited 2S1G and TAS films appear amorphous and smooth with no porous structure and have neither columnar nor granular microstructure.

The micro-structural characteristics of both 2S1G and TAS films were found preserved at the beginning of the aging experiments. The same observations were made also for TAS films exposed for 6 months to darkness and argon atmosphere (TAS, Fig. 4(c)). Under these conditions, the surface of the 2S1G film develops few isolated crystallites (2S1G, Fig. 4(c)). This effect could be linked to the increase of the optical band-gap value of this film by $\Delta E_{opt} = +0.05$ eV (Table 2) while TAS film did not present a ΔE_{opt} shift in same condition of aging. In any case, the combination of darkness with argon atmosphere seems to be an effective way for preventing chalcogenide films from premature aging.

Indeed, it was found for both TAS and 2S1G films that exposure to light and air atmosphere leads to micro-crystal formation on the surface. As seen in Fig. 4(b), this effect is more pronounced for the TAS film where a large concentration of micro-crystals has developed. Similar observations are made in the SEM image of a 1.5 μm TAS film depicted in Fig. 5. Previous studies on exposed $As_{40}S_{30}Se_{30}$ chalcogenide layer [52] and Ag(Cu)–As_2Se_3 films[53] showed the formation of As_2O_3 micro-crystals on the surface of the exposed films. This formation certainly follows mechanism close to those observed in As_2S_3 film for which photoinduced breakage of As–As bonds reacting with water and oxygen occurs at least at the surface of the film. In case of TAS EBD films, such homopolar As–As bonds

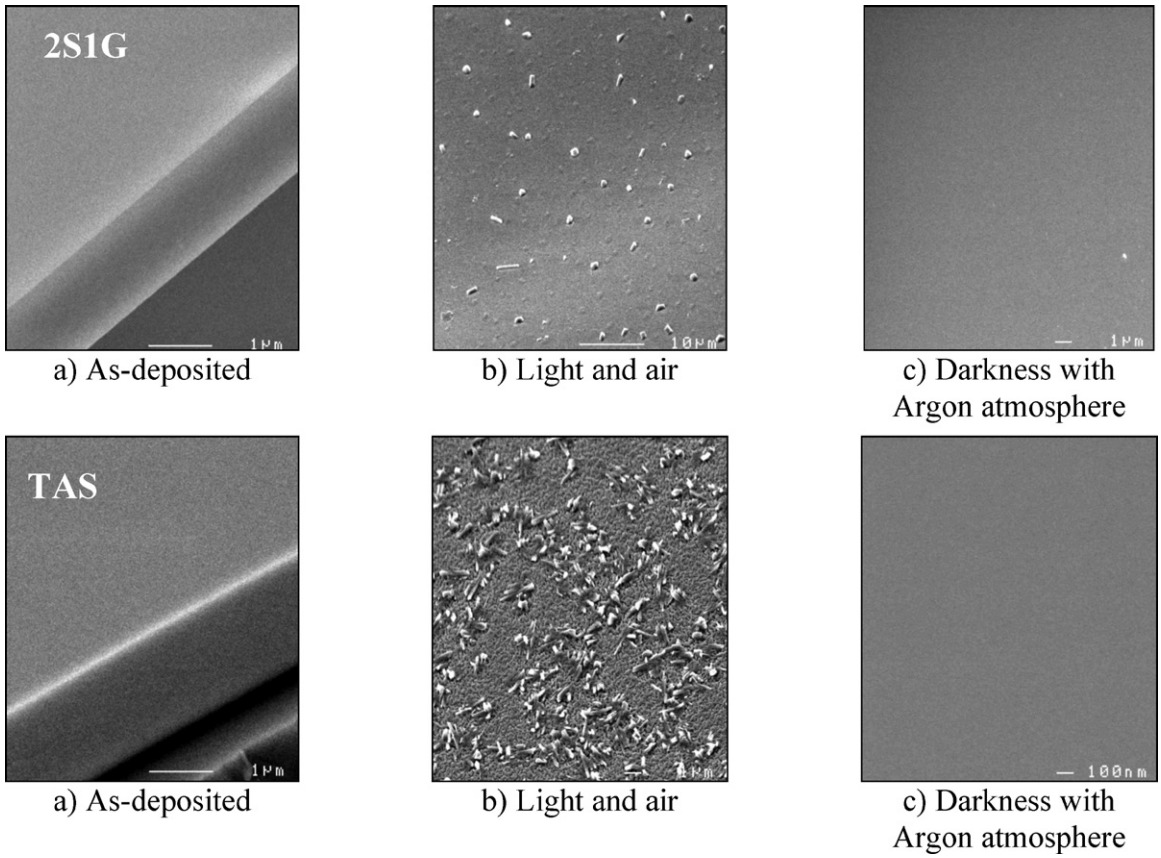

Fig. 4. SEM images of $Ge_{15}Sb_{20}S_{65}$ (a) and $As_{30}Se_{50}Te_{20}$ (b) EBD film as-deposited and exposed to light with air atmosphere or darkness with Argon atmosphere during 6 months.

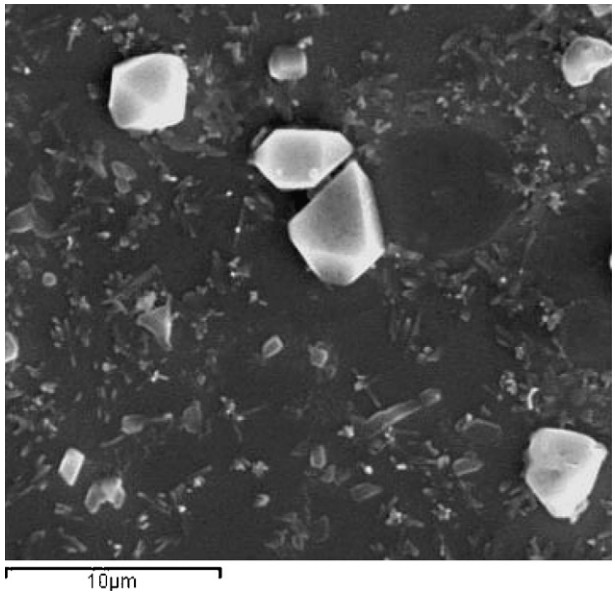

Fig. 5. SEM image of the surface of an exposed to light and air $As_{30}Se_{50}Te_{20}$ film with micro-crystals of As_2O_3.

were not revealed by vibrational spectroscopies for which Se–Se and Se–Te seems to be the preferential chalcogen-chalcogen bonds. The sensitivity of many chalcogenides to oxidation and hydrolysis exposed to light is well known [42]. Analyse by energy dispersive spectroscopy (EDS) of micro-crystallites on TAS film shows clearly an increase of oxygen in high proportion and decrease of selenium and tellurium compare to film composition, which permit to conclude to the formation of As_2O_3 micro-crystals also on the surface of the exposed TAS films. Both photo-oxidation and photo-hydrolysis effects could take place and explain the formation of this new As_2O_3 phase on the film surface.

Compared to TAS film, the oxidation of 2S1G film is less important as seen by the growth of small particles on the surface (see 2S1G, Fig. 4(b)). Kohoutek et al. [54] have reported the formation of As_2O_3 crystals onto As–S film surface as result of oxidation after exposure of air, while the introduction of few percent of Sb allowed preventing such behavior onto As–Sb–S film surface. Photo-oxidation under irradiation at 633 nm was observed by Cardinal et al. on germanium–sulfide films for which oxygen diffusion most probably occurs from the top of the film [50]. According to Tanaka et al. the formation of GeO_2 crystals by illumination could not be expected on the surface of the Ge based films [49]. They suggested that stoichiometric bulk glass GeS_2 is almost entirely constituted of heteropolar bonds in contrast with the as-evaporated film which the presence of homopolar bonds and dangling bonds are reported. Following light exposure in air, these Ge–Ge bridges or dangling bonds in lower proportion lead to formation of Ge–O–Ge bonds and photobleaching in GeS_2 films [49]. It is also worth noting that a recent study on oxysulfide glasses in the system Ge–Ga–As–S(O) has shown a preference of Ga to form Ga-oxysulfide units. The percentage of Ga atoms bonded to O was larger compared to that of Ge and As and the weakness of Ga–S compared to Ge–S and As–S bonds was proposed to explained this behavior. Nevertheless in our $Ge_{15}Sb_{20}S_{65}$ film, germanium atoms might be coordinated with both sulfur and oxygen and the formation of Ge–O could be related to the presence of tetrahedral units such as GeO_3S, GeO_2S_2 or $GeOS_3$ in agreement with Maurel et al. [50,51]. Such a tendency of Ge atoms could provide a mechanism for incorporating in the glassy network the diffusing oxygen atoms,

and, consequently, a way of reducing formation of oxidation crystallised products on the aged film surface. The photo-oxidation of TAS film seems to be more important at the surface of the film with oxide crystal grown than diffusion and reaction with the glassy network how it is suggested by the photodarkening of the film. These first conclusions should be study in more detail in order to determine the diffusion of oxygen into the film or photo-oxidation and photo-hydrolysis reaction limited at the film surface considering composition variation.

4. Conclusions

As chalcogenide EBD films can be used in the field of narrow bandpass filters (NBFs) in the near-infrared and mid-infrared region, omnidirectional reflectors cladding, all-optical signal processing devices or opto-chemical sensors, it is important to explore alterations of their optical properties and morphological characteristics during natural aging experiments. For this study, $Ge_{25}Sb_{10}S_{65}$ (2S1G) and $As_{30}Se_{50}Te_{20}$ (TAS) amorphous chalcogenides have been synthesised as bulk glasses in sealed silica tubes and as thin films by electron-beam deposition. The structure of thin films was compared to that of bulk glasses by employing IR and Raman spectroscopy. The results showed very similar network organization in bulk glass and thin film states, with small structural variations in EBD films arising mainly from compositional changes during deposition from bulk glass targets.

The photosensitivity of TAS and 2S1G layers was studied following the evolution of their band-gap during aging. After 6 months exposure to light and air atmosphere, the transmittance curves were found shifted toward shorter (photobleaching) and longer wavelengths (photodarkening) for 2S1G and TAS films, respectively. The optical band-gap values for both chalcogenide films have been determined as a function of aging time, and the results demonstrate the photosensitivity of these chalcogenide films.

Evidence for a photo-oxidation process limited on the surface of TAS films has been presented by following the evolution of SEM images, which show the growth of micro-crystals attributed to arsenic trioxide. Degradation of 2S1G films by formation of crystals on the film surface has been also observed, but the degree of this phenomenon is much smaller than that found for TAS films. The photobleaching observed for 2S1G EBD films could be related to diffusion of oxygen into the film reacting with the glass network. Therefore, the reaction of oxygen with germanium present in this sulfide film could lead to formation of oxysulfide compositions in the film, and thus, compared to TAS, to a less pronounced microcrystal formation on the surface during aging.

Acknowledgements

Partial support of this work by the EC (Grant No. MTKD-CT-2006-042301) is gratefully acknowledged. Funding from ADEME and BRGM (France) supported this project.

References

[1] M. Cathelinaud, V. Nazabal, F. Charpentier, J.L. Adam, K. Fedus, G. Boudebs, M. Chauvet, G. Fanjou, K.P. Huy, T. Billeton, S.P. Gorza, W.D. Shen, Chin. Opt. Lett. 8 (2010) 1–3.
[2] W.D. Shen, M. Cathelinaud, M.D. Lequime, F. Charpentier, V. Nazabal, Opt. Express 16 (2008) 373–383.
[3] S.D. Hart, G.R. Maskaly, B. Temelkuran, P.H. Prideaux, J.D. Joannopoulos, Y. Fink, Science 296 (2002) 510–513.
[4] H.E. Kondakci, M. Yaman, O. Koylu, A. Dana, M. Bayindir, Appl. Phys. Lett. 94 (2009).
[5] K. Richardson, L. Petit, N. Carlie, B. Zdyrko, I. Luzinov, J. Hu, A. Agarwal, L. Kimerling, T. Anderson, M. Richardson, J. Nonlinear Opt. Phys. Mater. 19 (2010) 75–99.
[6] A Ganjoo, H. Jain, C. Yu, J. Irudayaraj, C.G. Pantano, J. Non-Cryst. Solids 354 (2008) 2757–2762.
[7] M.D. Pelusi, F. Luan, S. Madden, D.Y. Choi, D.A. Bulla, B. Luther-Davies, B.J. Eggleton, IEEE Photonics Technol. Lett. 22 (2010) 3–5.
[8] B. Luther-Davies, D. Bulla, R.P. Wang, A. Prasad, S. Madden, D.Y. Choi, 2009 IEEE Leos Annual Meeting Conference Proceedings, vols. 1 and 2, 2009, pp. 402–403.
[9] V. Nazabal, M. Cathelinaud, W. Shen, P. Nemec, F. Charpentier, H. Lhermite, M.-L. Anne, J. Capoulade, F. Grasset, A. Moreac, S. Inoue, M. Frumar, J.-L. Adam, M. Lequime, C. Amra, Appl. Opt. 47 (2008) C114–C123.
[10] M. Frumar, H. Ticha, M. Vlcek, J. Klikorka, L. Tichy, Czech J. Phys. 31 (1981) 441.
[11] D.A. Turnbull, J.S. Sanghera, V.Q. Nguyen, I.D. Aggarwal, Mater. Lett. 58 (2004) 51–54.
[12] F. Hulderman, J.S. Sanghera, J.D. Mackenzie, J. Non-Cryst. Solids 127 (1991) 312–322.
[13] K. Ogusu, Y. Hosokawa, S. Maeda, M. Minakata, H. Li, J. Non-Cryst. Solids 351 (2005) 3132–3138.
[14] E. Marquez, J.M. Gonzalez-Leal, R. Jimenez-Garay, M. Vlcek, Thin Solid Films 396 (2001) 183–190.
[15] J.T. Bloking, S. Krishnaswami, H. Jain, M. Vlcek, R.P. Vinci, Opt. Mater. 17 (2001) 453–458.
[16] E.I. Kamitsos, Phys. Rev. B 53 (1996) 14659.
[17] E.I. Kamitsos, Y.D. Yiannopoulos, C.P. Varsamis, H. Jain, J. Non-Cryst. Solids 222 (1997).
[18] E.I. Kamitsos, M. Dussauze, C.P.E. Varsamis, P. Vinatier, Y. Hamon, J. Phys. Chem. C 111 (2007) 8111–8119.
[19] M. Dussauze, A. Giannoudakos, L. Velli, C.P.E. Varsamis, M. Kompitsas, E.I. Kamitsos, J. Chem. Phys. 127 (2007).
[20] E.I. Kamitsos, M. Dussauze, C.P.E. Varsamis, Phys. Chem. Glasses 49 (2008) 118–126.
[21] G. Lucovsky, F.L. Galeener, R.C. Keezer, R.H. Geils, H.A. Six, Phys. Rev. B 10 (1974) 5134–5146.
[22] K. Murase, T. Fukunaga, K. Yakushiji, T. Yoshimi, I. Yunoki, J. Non-Cryst. Solids 59-6 (1983) 883–886.
[23] P. Boolchand, J. Grothaus, M. Tenhover, M.A. Hazle, R.K. Grasselli, Phys. Rev. B 33 (1986) 5421–5434.
[24] E.I. Kamitsos, J.A. Kapoutsis, G.D. Chryssikos, G. Taillades, A. Pradel, M. Ribes, J. Solid State Chem. 112 (1994) 255–261.
[25] S. Sugai, Phys. Rev. B 35 (1987) 1345.
[26] I. Watanabe, S. Noguchi, T. Shimizu, J. Non-Cryst. Solids 58 (1983) 35.
[27] M. Kato, S. Onari, T. Arai, Jpn. J. Appl. Phys. Part 1-Regular Papers Short Notes Rev. Papers 22 (1983) 1382–1387.
[28] I.P. Kotsalas, D. Papadimitriou, C. Raptis, M. Vlcek, M. Frumar, J. Non-Cryst. Solids 226 (1998) 85–91.
[29] G. Delaizir, M. Dussauze, V. Nazabal, P. Lecante, M. Dolle, P. Rozier, E.I. Kamitsos, P. Jovari, B. Bureau, J. Alloys Compd. 509 (2011) 831–836.
[30] G. Lucovsky, Phys. Rev. B 6 (1972) 1480–1489.
[31] G. Lucovsky, R.M. Martin, J. Non-Cryst. Solids 8–10 (1972) 185–190.
[32] G. Lucovsky, A. Mooradia, W. Taylor, G.B. Wright, R.C. Keezer, Solid State Commun. 5 (1967) 113–117.
[33] T. Ohsaka, J. Non-Cryst. Solids 17 (1975) 121–128.
[34] T. Mori, S. Onari, T. Arai, Jpn. J. Appl. Phys. 19 (1980) 1027–1031.
[35] M.S. Iovu, E.I. Kamitsos, C.P.E. Varsamis, P. Boolchand, M. Popescu, J. Optoelectron. Adv. Mater. 7 (2005) 1217–1221.
[36] A. Mendoza-Galvan, E. Garcia-Garcia, Y.V. Vorobiev, J. Gonzalez-Hernandez, Microelectron. Eng. 51–52 (2000) 677–687.
[37] V.Q. Nguyen, J.S. Sanghera, J.A. Freitas, I.D. Aggarwal, I.K. Lloyd, J. Non-Cryst. Solids 248 (1999) 103–114.
[38] J. Hu, X. Sun, A.M. Agarwal, J.F. Viens, L.C. Kimerling, L. Petit, N. Carlie, K.C. Richardson, T. Anderson, J. Choi, M. Richardson, J. Appl. Phys. 101 (2007).
[39] J. Tauc, in: J. Tauc (Ed.), Amorphous and Liquid Semiconductors, Plenum, New York, 1974.
[40] A. Ganjoo, R. Golovchak, J. Optoelectron. Adv. Mater. 10 (2008) 1328–1332.
[41] W.D. Shen, M. Cathelinaud, M. Lequime, V. Nazabal, X. Liu, Opt. Commun. 281 (2008) 3726–3731.
[42] M. Frumar, B. Frumarova, T. Wagner, P. Nemec, in: A.V. Kolobov (Ed.), Photo-Induced Metastability in Amorphous Semiconductors, Wiley-WCH, Weinheim, Germany, 2003, pp. 23–44.
[43] R. Ston, M. Vlcek, H. Jain, J. Non-Cryst. Solids 326 (2003) 220–225.
[44] A. Zakery, S.R. Elliott, J. Non-Cryst. Solids 330 (2003) 1–12.
[45] M. Vlcek, M. Frumar, A. Vidourek, J. Non-Cryst. Solids 90 (1987) 513–516.
[46] E.N.B.A.V. Povolotskiy, T. Yu Ivanova, A.A. Manshina, Laser Phys. Lett. 3 (2006) 190–194.
[47] S.H. Messaddeq, M.S. Li, S. Inoue, S.J.L. Ribeiro, Y. Messaddeq, Appl. Surf. Sci. 252 (2006) 8738–8744.
[48] S.H. Messaddeq, V.R. Mastelaro, M. Siu Li, M. Tabackniks, D. Lezal, A. Ramos, Y. Messaddeq, Appl. Surf. Sci. 205 (2003) 143–150.
[49] K. Tanaka, Y. Kasanuki, A. Odajima, Thin Solid Films 117 (1984) 251–260.
[50] C. Maurel, T. Cardinal, P. Vinatier, L. Petit, K. Richardson, N. Carlie, F. Guillen, M. Lahaye, M. Couzi, F. Adamietz, V. Rodriguez, F. Lagugne-Labarthet, V. Nazabal, A. Royon, L. Canioni, Mater. Res. Bull. 43 (2008) 1179–1187.
[51] C. Maurel, L. Petit, M. Dussauze, E.I. Kamitsos, M. Couzi, T. Cardinal, A.C. Miller, H. Jain, K. Richardson, J. Solid State Chem. 181 (2008) 2869–2876.
[52] E. Márquez, J.M. González-Leal, R. Jiménez-Garay, M. Vlcek, Thin Solid Films 396 (2001) 184–191.
[53] K. Ogusu, T. Hagihara, Y. Hosokawa, M. Minakata, J. Non-Cryst. Solids 353 (2007) 1216–1220.
[54] T. Kohoutek, T. Wágner, M. Vlcek, M. Vlcek, M. Frumar, J. Non-Cryst. Solids 351 (2005) 2205–2209.